ORIGINAL CONTRIBUTION

CrossMark

Phase behavior of cholesterol-containing binary membrane of an ether-linked phospholipid, dihexadecylphosphatidylcholine

Nobutake Tamai[1] · Maiko Uemura[2] · Takuya Izumikawa[2] · Masaki Goto[1] · Hitoshi Matsuki[1] · Shoji Kaneshina[2]

Abstract

The thermotropic phase behavior of the cholesterol (Chol)-containing binary membrane of dihexadecylphosphatidylcholine (DHPC) was investigated as a function of the mole fraction of Chol X_{ch} by DSC and fluorescence spectroscopy using 6-propionyl-2-(N,N-dimethylamino)naphthalene (Prodan). The main-transition enthalpy ΔH_m was almost constant at $X_{ch} <$ ca. 0.05, but it decreased almost linearly with increasing X_{ch} above 0.05 until it reached 0 at $X_{ch} =$ ca. 0.50, suggesting that the interaction between DHPC and Chol is relatively weaker than that between dipalmitoylphosphatidylcholine (DPPC) and Chol. The Prodan fluorescence spectra changed depending on the phase state, which was characterized by the wavelength at the emission maximum. Particularly, the two-phase state of the interdigitated ($L_\beta I$) and non-interdigitated (L_β) gel was sensitively detected as the superposition of the two elementary spectra corresponding to each phase state, allowing us to explain the X_{ch} dependent non-linear behavior of the Chol-induced L_β phase by introducing a proportionality factor $\xi(X_{ch})$ and by assuming a simple probabilistic process. By comparing the phase diagram constructed for the DHPC–Chol binary membrane with that for the DPPC–Chol binary bilayer, a difference was observed in the minimum X_{ch} value for the entire formation of the liquid ordered (L_o) phase. This difference could be explained in terms of the hydrophobic mismatch at the bilayer midplane by taking into account the difference in the capability of hydrogen bonding with the 3β-OH group of Chol due to the presence or absence of the carbonyl oxygens at the glycerol backbone.

Keywords Cholesterol · Dihexadecylphosphatidylcholine · Interdigitation · Liquid ordered phase · Phase diagram · Peritectic point

Introduction

One of the phospholipid species that have been most often used in model membrane studies is dipalmitoylphosphatidylcholine (DPPC), which consists of a polar headgroup of phosphocholine (PC) and two palmitoyl chains attached to the glycerol backbone by ester linkages. The DPPC bilayer membrane exhibits several types of phase transitions with variations

in the surroundings: it undergoes the pretransition at ca. 34 °C and the main transition at ca. 42 °C under the atmospheric pressure [1, 2]. The former and latter transitions correspond to the conversion from a lamellar gel (L_β') phase to a ripple gel (P_β') phase and the conversion from the P_β' phase to a liquid crystalline (L_α) phase, respectively. On the other hand, some kinds of phospholipids are known to be capable of forming molecular aggregates with non-bilayer structures. Dihexadecylphosphatidylcholine (DHPC) is one of those phospholipids. DHPC has the same chemical structure as DPPC except that the two hydrocarbon chains of the DHPC molecule are attached to the glycerol backbone by ether linkages (Fig. 1). Hence, DHPC is often categorized as an ether-linked PC lipid while DPPC is an ester-linked PC lipid. Seemingly, the DHPC membrane shows similar thermotropic phase behavior to that of the DPPC bilayer membrane: it undergoes the pretransition at ca. 35 °C and the main transition at ca. 44 °C under atmospheric pressure [3–6]. However, the pretransition of the DHPC membrane is not the L_β'/P_β'

✉ Hitoshi Matsuki
matsuki@tokushima–u.ac.jp

[1] Department of Bioengineering, Division of Bioscience and Bioindustry, Graduate School of Technology, Industrial and Social Sciences, Tokushima University, 2-1 Minamijosanjima-cho, Tokushima 770-8513, Japan

[2] Department of Biological Science and Technology, Faculty of Engineering, Tokushima University, 2-1 Minamijosanjima-cho, Tokushima 770-8506, Japan
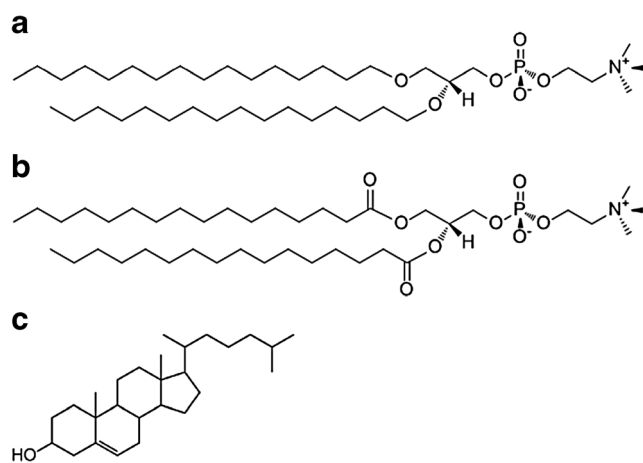
Fig. 1 Chemical structures of (a) DHPC, (b) DPPC, and (c) Chol

transition but the transition from a so-called interdigitated gel (L$_\beta$I) phase to the P$_{\beta}$′ phase. In the L$_\beta$I phase, the hydrocarbon chains of the DHPC molecules in the two opposing monolayers of a bilayer alternately interpenetrate beyond the bilayer midplane [4, 7]. Several previous studies [8, 9] have shown that a notable difference between the DPPC and the DHPC bilayer membrane can be seen in the structure of water in hydration shells and that the interaction between adjacent polar headgroups is weaker in the DHPC membrane than in the DPPC bilayer. In general, therefore, it is thought that weaker interaction in the hydrophilic region of the bilayer membrane is related to the propensity of DHPC to form the interdigitated structure.

In recent model-membrane studies, binary and ternary phospholipid bilayer membranes containing cholesterol (Chol) have often been used. Chol is a major component of the plasma membrane and is also thought to be essentially relevant to the formation of functional microdomains called lipid rafts [10]. Ipsen et al. [11] predicted the phase behavior of the DPPC–Chol binary bilayer membrane by constructing the compositional phase diagram on the basis of theoretical calculations. Their phase diagram suggested several significant features: a third phase that is distinguished from a solid ordered (S$_o$) phase like L$_{\beta}$′ and P$_{\beta}$′ phase and a liquid disordered (L$_d$) phase like L$_\alpha$ phase occurs in a higher Chol composition region (> ca. 30 mol%) and two-phase regions of the L$_d$ (or S$_o$) and the third phase appear in an intermediate Chol composition region. The third phase was termed liquid ordered (L$_o$) phase, where constituent lipids have higher conformational order of the acyl chains than in the L$_d$ phase and relatively faster lateral diffusion than in the S$_o$ phase. These theoretical predictions were experimentally confirmed by Vist and Davis [12]. We also have recently reported the temperature (T)–Chol mole fraction (X_{ch}) phase diagrams for the Chol-containing binary bilayer membranes of a series of linear saturated diacylphosphatidylcholines with different acyl chain length n (i.e., CnPC, n = 14–18) [13–15]. Our phase diagrams

suggested several interesting features about the phase behavior of these binary bilayer membranes. One is that the phase behavior of those binary bilayer membranes was quite similar to typical peritectic melting behavior, suggesting that Chol tends to form molecular complexes with its surrounding phospholipids within the binary bilayer membranes. Another is that biphasic n-dependence was observed for the X_{ch} values at which the pretransition is abolished. These features can be reasonably explained by applying the so-called superlattice view (i.e., regular distribution of Chol within the binary bilayer membrane) [16].

On the other hand, very few studies have been conducted on the phase behavior of Chol-containing binary membrane of ether-linked PC lipids like DHPC [17] despite the fact that they are peculiar in their capability of forming the interdigitated structure without any inducer. In this study, we investigated the phase transitions of the DHPC–Chol binary membrane by means of differential scanning calorimetry (DSC) and fluorescence spectroscopy using 6-propionyl-2-(N,N-dimethylamino)naphthalene (Prodan) as a membrane probe [18, 19] to construct the T–X_{ch} phase diagram for the DHPC–Chol binary membrane. Since different structures of lipid membranes are generally dealt with as different phases, constructing a compositional phase diagram is a suitable way to examine the overall effect of Chol on the lateral organization of lipid membranes. The first aim of this study is to clarify similarities and differences in the phase behavior of the cholesterol-containing binary membranes of DHPC and DPPC and to discuss how those similarities and differences are associated with the difference in the chemical structure between DHPC and DPPC. As described above, the difference in the chemical structure between DHPC and DPPC is very small, but it can be a non-trivial factor when considering the interaction with Chol, because the carbonyl group in DPPC can function as a hydrogen bond acceptor. In fact, an MD simulation study [20] has shown that the formation of hydrogen bonding networks in the headgroup region via the 3β-OH groups of Chol plays a crucial role in the formation of 1:1 or 1:2 complexes of Chol and DPPC, which leads to the occurrence of membrane domains.

The second aim of this study is to examine the effect of Chol incorporation on the formation of the interdigitated structure in the DHPC membrane. A previous X-ray scattering and calorimetric study [21] has revealed that Chol incorporated into the DHPC membrane has a perturbing effect on the chain interdigitation and induces non-interdigitated (i.e., bilayer) gel structure, and also that the interdigitated and non-interdigitated gel state can coexist until the chain interdigitation is completely abolished at the Chol concentration of 5 mol% (X_{ch} = 0.05). However, this Chol concentration is not consistent with their own DSC result, which shows that the pretransition persists up to 10 mol% (X_{ch} = 0.10). Then we re-examined the Chol effect on the chain interdigitation by

applying Prodan fluorescence technique to consider the process of the conversion from the interdigitated gel to the non-interdigitated gel induced by the incorporation of increasing amount of Chol. The Prodan fluorescence technique can sensitively detect the conversion from the interdigitated gel to the non-interdigitated gel phase as a clear shift of the wavelength at the emission maximum (λ_{max}) [22].

Experimental

A synthetic phosphatidylcholine, DHPC (1,2-di-O-hexadecanoyl-sn-glycero-3-phosphocholine, purity > 99%), was purchased from Avanti Polar Lipids (Alabaster, AL) and cholesterol (5-cholesten-3β-ol, purity $\geq$ 99%) was from Sigma-Aldrich Co. (St. Louis, MO). The chemical structures of DHPC and Chol, along with that of DPPC, are shown in Fig. 1. The fluorescent probe of Prodan (6-propionyl-2-(N,N-dimethylamino)naphthalene) was purchased from Molecular Probes Inc. (Eugene, OR). All the materials were used without further purification. Water was distilled twice from dilute alkaline permanganate solution to prepare all sample solutions. Aqueous dispersions of multilamellar vesicles containing Chol were prepared by the following procedure. First, appropriate amounts of stock solutions of Chol/chloroform and Prodan/ethanol were added to a weighed amount of phospholipid powder. Second, the mixed solution was dried in vacuum to remove all residual solvents. Finally, a given amount of distilled water was added to the resulting dry film, and subsequently, the heterogeneous aqueous mixture was vortexed and sonicated for a few minutes at about 50 °C to obtain a homogeneously translucent aqueous dispersion. The concentrations of the phospholipid and Prodan were fixed at 1 mmol kg^{-1} and 2 μmol kg^{-1} (i.e., the molar ratio of Prodan to phospholipids is 1:500), respectively [19]. We have confirmed that such a slight amount of Prodan has no significant effect on the thermotropic phase behavior of phospholipid membranes [19]. The mole fraction of Chol X_{ch} in a binary membrane defined as

$$X_{ch} = m_{ch}/(m_{ch} + m_{DHPC}) = n_{ch}/(n_{ch} + n_{DHPC}) \quad (1)$$

was varied in the range from 0 to 0.50. Here, m_{ch}, m_{DHPC}, n_{ch}, and n_{DHPC} denote the molalities of Chol and DHPC and the number of moles of Chol and DHPC, respectively.

Fluorescence spectroscopic measurements were performed using an F-3010 fluorescence spectrophotometer (Hitachi High-Technology Corp., Tokyo) at constant temperatures ranging from 5 to 80 °C. The temperature was controlled within an accuracy of 0.1 °C by circulating thermostated water from a temperature-regulated water bath. A light with the wavelength of 361 nm was used for the excitation of the membrane probe Prodan and the emission spectra were acquired in the range of 400–600 nm. Data analyses were carried out by using Excel 2013 (Microsoft) and Kaleida graph ver. 4.0 (Synergy software).

DSC measurements were carried out using a high-sensitivity differential scanning calorimeter MCS (MicroCal, Northampton, MA). DSC thermograms were recorded in the temperature range of 10–80 °C at the heating rate of 0.33 °C min^{-1} by using water as a reference solution. Each DSC measurement was composed of two heating scans, namely a first heating scan and a second heating scan performed immediately after the first scan was completed, and at least two independent DSC measurements were applied to each sample solution. A transition temperature was determined as the temperature at the top of an endothermic peak and an enthalpy change with a transition ΔH was estimated by integrating an endothermic peak using Excel 2013 as well as data-analyzing software ORIGIN ver. 7.0. In the analysis of DSC data using Excel 2013, baseline subtraction was done to obtain a ΔH value by producing a baseline by least-squares regression with a polynomial function.

Results

DSC measurements

Figure 2(a) shows the overall DSC thermograms for the DHPC–Chol binary membranes with different Chol concentrations (X_{ch} = 0–0.45) to see the rough tendency of how the endothermic peak of the main transition changed with increasing X_{ch}. For the pure DHPC membrane (i.e., X_{ch} = 0, curve a-1), a small endothermic peak, arising from the pretransition, and a large sharp endothermic peak, from the main transition, were clearly observed at 34 and at 44 °C, respectively, which is consistent with previous studies [3–7]. As X_{ch} increased, the main-transition peak gradually increased in width but markedly decreased in height, and as a result, it became smaller as a whole. At X_{ch} = 0.20, only a very broad peak was observed (curves a-5 and a-6). This broad peak also became broader and smaller with further increases in X_{ch} and eventually became completely undetectable at X_{ch} = 0.50. The peak-top temperature was also changed slightly with X_{ch}: it shifted slightly to lower temperatures with increasing X_{ch} up to ca 0.15, whereas it shifted gradually to higher temperatures with increasing X_{ch} above 0.15. Figure 2(b) shows the magnified view of the DSC thermograms in the vicinity of the pretransitions at every 0.02 up to X_{ch} = 0.10. The endothermic peak of the pretransition also became smaller and broader with increasing X_{ch} and finally it became undetectable at X_{ch} > 0.10. This X_{ch} value is slightly higher than that for the DPPC–Chol binary bilayer (i.e., 0.07–0.08 [15]) and much higher than that for the DSPC–Chol binary bilayer (i.e., 0.035–0.04 [13]). Parallel to this change in the peak shape, the peak top progressively shifted to lower temperatures with increasing X_{ch}.

Fig. 2 Overall (a, c) and magnified (b, d) view of DSC thermograms for a series of DHPC–Chol binary membranes with different Chol concentrations (X_{ch}). Schematic illustration represents the molecular arrangements in interdigitated ($L_\beta I$) phase, ripple gel (P_β') phase, and liquid crystalline (L_α) phase of pure DHPC membrane. (a) Overall behavior of the Chol effect on the main transition. Curves 6–11 have been 20-fold magnified in the y-axis direction to improve visibility. Note that curves 5 and 6 are the same DSC thermogram. (b) Chol effect on the pretransition. (c, d) Change in the shape of main-transition peak with increasing X_{ch}. Curves 4–6 have been 5-fold magnified in the y-axis direction relative to curves 1–3. Note that curves 3 and 4 are the same DSC thermogram
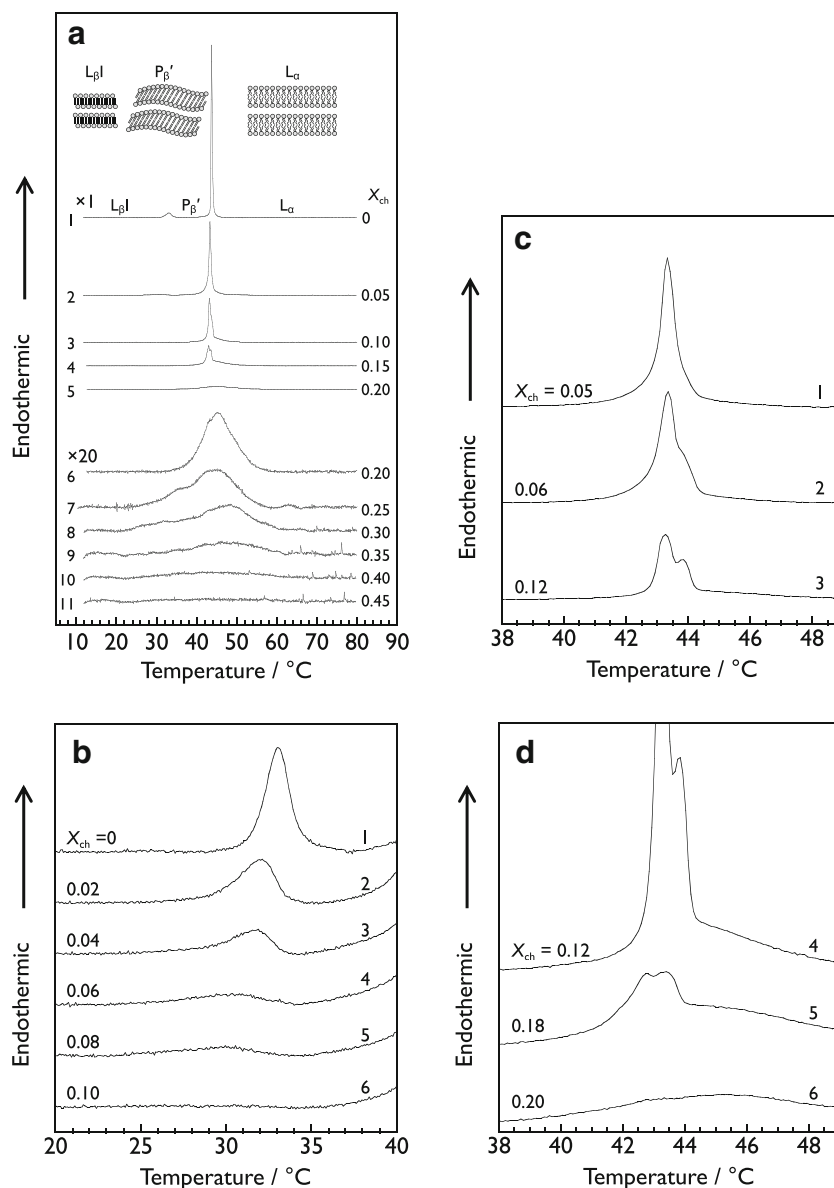
In Fig. 2(c, d), the magnified view of the main-transition peaks at several specific X_{ch} in the intermediate X_{ch} region ($0.05 \leq X_{ch} \leq 0.20$) is shown to see in more detail how the line shape of the main-transition peak changes with the variation in X_{ch}. An obviously asymmetric peak was observed at $X_{ch} = 0.06$ (curve c-2), though the main-transition peak observed at $X_{ch} = 0.05$ (curve c-1) was almost symmetric. This peak asymmetry is apparently attributable to the presence of another non-negligible peak at a slightly higher temperature than that of the original main-transition peak. The heights of both original and second peak decreased with an increase in X_{ch}. The second peak could be comparatively more clearly observed in the DSC thermogram at $X_{ch} = 0.12$ (curve c-3). From its line shape, the second peak seems almost as sharp as the original main-transition peak. In addition, this

thermogram also shows that there is a slight mismatch between the heights of the baseline before and after the peaks, which suggests that there is a very broad peak as a third component that has a maximum at a temperature slightly higher than that of the second peak. This mismatch can be more clearly seen in the thermogram further magnified in the vertical direction (curve d-4 in Fig. 2(d)). This broad peak was relatively less affected by the increase in the X_{ch}, whereas the other two sharp peaks became noticeably smaller with an increase in X_{ch} (curve d-5). The two sharp peaks eventually became almost undetectable at $X_{ch} = 0.20$, and as a result, only the third broad peak remained as a detectable component (curve d-6). The DPPC–Chol binary bilayer membrane also exhibited similar behavior in almost the same X_{ch} range except that only two component peaks (i.e., a sharp and a broad

component peak) were observed [15]. As will be described later, this X_{ch}-dependent complicated change in the DSC endothermic peaks is probably related to the heterogeneous distribution of Chol within the binary membrane due to two-phase coexistence.

From the DSC results, we were able to determine several typical thermodynamic properties that characterize the main transition of a series of DHPC–Chol binary membranes with different Chol concentrations. Figure 3(a–c) shows the X_{ch} dependence of the main-transition enthalpy (ΔH_m), the main-transition temperature (T_m), and the peak width at half height of the main-transition peak ($\Delta T_{1/2}$), respectively. For comparison, the same kinds of data obtained in our previous studies for the binary bilayers of DPPC–Chol [15] and DSPC–Chol [13] are also plotted together in each of Fig. 3(a–c). As seen from Fig. 3a, the ΔH_m value of the DHPC–Chol binary membrane was almost constant at $X_{ch} \leq 0.05$, which is evidently different from the behavior for the binary bilayers of the other two ester-linked PCs in the same X_{ch} range. It is well known that the main transition is associated with the *trans–gauche* conformational change of the hydrocarbon chains of the constituent lipid molecule [23] and also that Chol incorporated into a phospholipid membrane has an inhibitory effect on this conformational change of its surrounding lipid molecules [24]. Taking this into account, this invariance of the ΔH_m value observed at $X_{ch} \leq 0.05$ can be interpreted as indicating that virtually no DHPC molecules are restricted from the *trans–gauche* conformational change at the main transition in the presence of such a small amount of Chol. The difference in the behavior of ΔH_m in this X_{ch} region between

DHPC and the other ester-linked PCs may suggest that the phospholipid–Chol interaction is weaker within the Chol-containing binary membrane of DHPC than within those of ester-linked PCs.

With a further increase in X_{ch}, the ΔH_m value decreased almost linearly and became 0 finally at an X_{ch} between 0.45 and 0.50. Taking the above inhibitory effect of Chol into account, this almost linear decrease in ΔH_m with X_{ch} can be considered to imply that the population of the DHPC molecules capable of causing the thermotropic *trans–gauche* conformational change decreases nearly in proportion to the number of the Chol molecules incorporated into the binary membrane. In addition, this linearity may suggest that Chol tends to be scattered uniformly over the entire membrane rather than to be localized to form a distinct region with extremely high concentration of Chol. Finally, the main transition is completely abolished when the *trans–gauche* conformational change of all the DHPC molecules within the binary membrane is completely suppressed by Chol incorporated into the membrane. The X_{ch} value of the abolition of the main transition ($X_{ch}*^{main}$) can be estimated from Fig. 3(a) at ca. 0.50 for the DHPC. This value is obviously higher than that for the DPPC–Chol binary bilayer (i.e., $X_{ch}*^{main} \sim 0.33$) but is close to that for the DSPC–Chol binary bilayer (i.e., $X_{ch}*^{main} \sim 0.50$). This difference may also be due to the fact that the DHPC–Chol interaction is weaker than the DPPC–Chol interaction.

T_m of the DHPC–Chol binary membrane, as shown in Fig. 3(b), decreased slightly with increasing X_{ch} in the low X_{ch} region. This seems to be similar to the X_{ch} dependence of T_m for the DPPC– and the DSPC–Chol binary bilayers. In
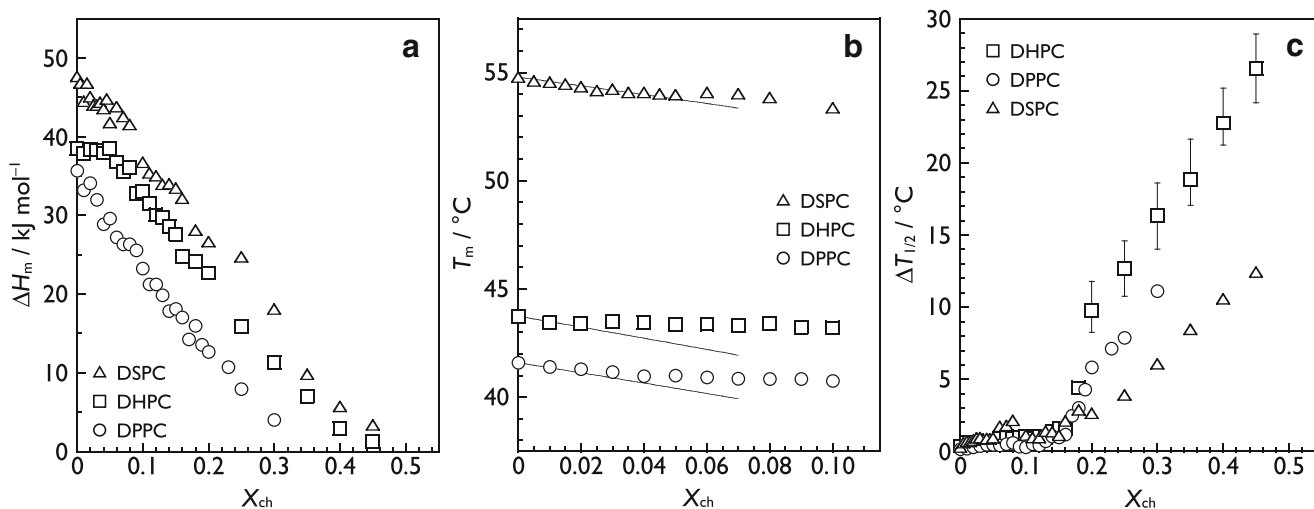

Fig. 3 Chol concentration (X_{ch}) dependence of (a) enthalpy change with main transition (ΔH_m), (b) main-transition temperature (T_m), and (c) peak width at half height ($\Delta T_{1/2}$) for DHPC–Chol binary membrane (square). The same results for the Chol-containing binary bilayer of DPPC (circle) and DSPC (triangle) obtained in the previous studies [13, 15] are also plotted for comparison. In (b), solid lines represent the calculated curve based on the general thermodynamic relation (Eq. (2))

this figure, the theoretical curve based on the following thermodynamic relation is also shown as a solid line for each binary membrane:

$$\ln(1-X_{\text{ch}}) = \frac{\Delta H_{\text{m}}°}{R}\left(\frac{1}{T_{\text{m}}} - \frac{1}{T_{\text{m}}°}\right) \quad (2)$$

Here, R is the gas constant, and $\Delta H_{\text{m}}°$ and $T_{\text{m}}°$ represent the enthalpy change and temperature of the main transition for the pure membrane (i.e., the values of ΔH_{m} and T_{m} at $X_{\text{ch}} = 0$), respectively. This equation predicts the extent of the depression of the main-transition temperature when the binary membrane can be regarded as an ideal mixture, where phospholipid and Chol molecules are completely miscible in a liquid crystalline state but are perfectly immiscible in a gel state. For the DHPC–Chol binary membrane, agreement between the experimental results and the theoretical prediction can be seen in the very dilute region (i.e., $X_{\text{ch}} <$ ca. 0.02). The DPPC–Chol binary bilayer also exhibited similar behavior (i.e., $X_{\text{ch}} <$ ca. 0.02), whereas the agreement was observed in a comparatively wider X_{ch} region (i.e., $X_{\text{ch}} <$ ca. 0.04) for the DSPC–Chol binary bilayer. This indicates that these binary membranes can be regarded as ideal binary mixtures in these very limited X_{ch} regions; that is, these kinds of phospholipids and Chol are almost completely immiscible in the gel state but ideally miscible in the liquid crystalline state. In the higher X_{ch} region, on the other hand, the experimental values of T_{m} became gradually higher than the theoretical prediction for each binary membrane with increasing X_{ch}. In general, the positive deviation from the theoretical prediction can be caused by either non-ideal mixing in the liquid crystalline state or imperfect immiscibility in the gel state, or both. Although it is quite difficult to accurately identify which effect is dominant, the deviation observed here seems to be attributable mainly to the latter reason, because, as will be described later, the distribution of Chol within the binary membrane in the gel state is expected to be rather heterogeneous, suggesting that the Chol and the DHPC molecules are partially miscible even in the gel state.

A notable feature of the X_{ch} dependence of $\Delta T_{1/2}$ (Fig. 3(c)) is that the dependence drastically changes in the vicinity of $X_{\text{ch}} = 0.15$: the $\Delta T_{1/2}$ value varied very slightly with X_{ch} below that Chol concentration, while it increased steeply with increasing X_{ch} above that concentration. As described above, the drastic change in the X_{ch} dependence of $\Delta T_{1/2}$ is due to the fact that the broad component peak becomes relatively dominant as compared to the sharp component peaks at $X_{\text{ch}} \geq$ ca. 0.15. Since $\Delta T_{1/2}$ is inversely related to the cooperativity of the transition in general [23, 25], the steep increase in $\Delta T_{1/2}$ at $X_{\text{ch}} \geq$ ca. 0.15 indicates that the intermolecular cooperativity at the chain-melting transition is markedly reduced with increasing X_{ch} in the higher X_{ch} region. As seen from Fig. 3(c), this is a common feature to the binary membranes of DHPC–, DPPC–, and DSPC–Chol. In our previous studies [14, 15], it

has been demonstrated that similar behavior is also observed for the other Chol-containing binary bilayers of CnPCs ($n = 14$, 15, and 17) in addition to DPPC (i.e., C16PC) and DSPC (i.e., C18PC), and we found that the L$_o$ phase begins to be formed within the binary bilayer as one of coexisting two phases at this common X_{ch} value of ca. 0.15 on the T–X_{ch} phase diagrams. This is also the case for the DHPC–Chol binary membrane, as will be confirmed later on the phase diagram.

In contrast to the qualitative similarity, an obvious difference in the values of $\Delta T_{1/2}$ can be seen in the higher X_{ch} region: the $\Delta T_{1/2}$ value increased to more than 25 °C for the DHPC–Chol binary membrane, while the main transition was abolished in the DPPC– and the DSPC–Chol binary bilayer before it reached 15 °C. This indicates that the incorporation of Chol produces much greater degree of reduction in the cooperativity of the main transition in the DHPC membrane than in the DPPC and the DSPC bilayers. The cooperativity of the main transition is a measure of how fast or how far the effect of the *trans–gauche* conformational change will propagate within the membrane when one constituent phospholipid molecule underwent the conformational change. In the case of binary membranes in a two-phase state, therefore, it would depend on long-range order of the lateral organization of the binary membrane rather than short-range molecular interactions including interactions between the same species. Therefore, the difference in the $\Delta T_{1/2}$ value may suggest that there is some difference in the size or morphology of the individual phase regions within the binary membrane in the two-phase state.

Prodan fluorescence

Figure 4(a) shows the Prodan fluorescence spectra $F(\lambda)$ (λ: wavelength) obtained for the DHPC membrane at different temperatures ranging from 5 to 50 °C. Each spectrum had a unique local maximum in the λ-range of 400–600 nm and the wavelength at the emission maximum (λ_{max}) slightly varied depending on the temperature. In our previous studies [19, 26–30], it has been shown for bilayer membranes of several ester-linked saturated PCs that there is a good correlation between the λ_{max} value and the membrane phase state: $\lambda_{\text{max}} = 480$–490 nm for the L$_\alpha$ phase, 430–440 nm for the L$_\beta'$ (or L$_\beta$), and the P$_{\beta}'$ phase and 500–510 nm for the L$_\beta$I phase. As seen from Fig. 4(a), Prodan in the DHPC membrane exhibited similar fluorescence behavior: the emission maximum can be seen at 500 nm (i.e., L$_\beta$I phase) below the pretransition temperature (ca. 34 °C) while that can be seen at 490 nm (i.e., L$_\alpha$ phase) above the main-transition temperature (ca. 44 °C). On the other hand, the λ_{max} value for the P$_{\beta}'$ phase (488 nm) was much higher compared to the case for the ester-linked saturated PC bilayers. This is presumably due to the difference in the location of the Prodan molecule along the depth of the bilayer membrane: it is located around the phosphate group in the

Fig. 4 (a) Prodan emission spectra $F(\lambda)$ obtained at different temperatures for DHPC membrane. (b) Temperature dependence of the wavelength at the maximum emission (λ_{max}) for DHPC membrane. (c) Temperature dependence of the intensity ratio $F(430)/F(490)$ for DHPC membrane
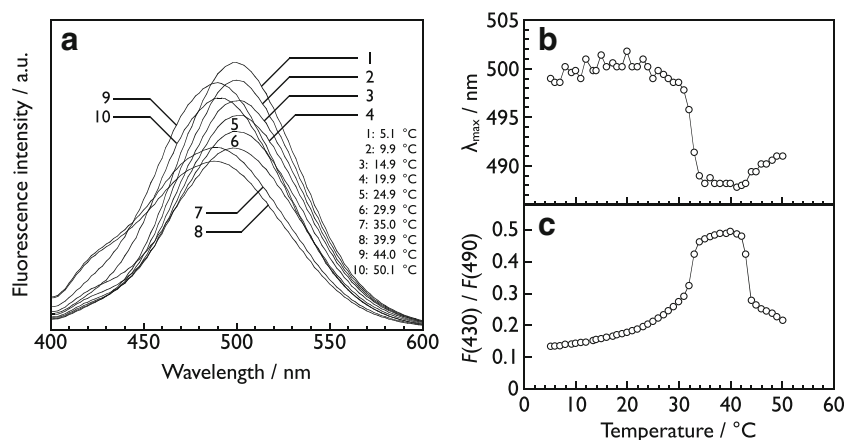
DHPC membrane, while it exists around the glycerol backbone in the bilayer membranes of ester-linked PCs [22].

To clarify the relationship between the variation in λ_{max} and the phase state of the DHPC membrane, the temperature dependence of λ_{max} is shown in Fig. 4(b). The λ_{max} value steeply decreased from ~500 to ~490 nm around the pretransition temperature and very slightly increased at the main-transition temperature, which means that these transition temperatures can be determined from the variation in λ_{max} for the DHPC membrane. In our previous studies, the intensity ratio of $F(430)/F(490)$ was also used for the observation of the bilayer phase transitions of ester-linked saturated PCs [15]. Similarly, the temperature dependence of this ratio for the DHPC membrane is shown in Fig. 4(c). The ratio increased at the pretransition temperature and decreased at the main-transition temperature, indicating that this ratio is also applicable to the detection of the phase transitions of the DHPC membrane. Although the characteristic λ_{max} value of the $L_\beta I$ phase is ca. 500 nm, we used the ratio $F(430)/F(490)$, and not $F(500)/F(490)$, as an index for the detection of the bilayer transition, because the two wavelengths of 490 nm and 500 nm are too close as compared to the width of each fluorescence peak.

Figure 5 shows the Prodan fluorescence spectra obtained at different temperatures for the DHPC–Chol binary membranes with various Chol concentrations. At $X_{ch} = 0.028$, the binary membrane exhibited relatively complicated spectral change with increasing temperature (Fig. 5(a)). The spectrum obtained at 5 °C showed two local maxima at ca. 430 and ca. 500 nm, suggesting that this spectrum consists of two elementary spectra superposed, each of which has a maximum in the vicinity of 430 or 500 nm (curve 1 in Fig. 5(a)). It is known that Chol tends to induce an L_β-like phase, in which the hydrocarbon chains of the constituent phospholipids are oriented almost parallel to the bilayer normal [31]. Considering that the characteristic λ_{max} value of the L_β phase is 430–440 nm, the appearance of the local maximum at ca. 430 nm indicates that the L_β phase was partially formed in the binary membrane.

The intensities at 430 and 500 nm increased and decreased with increasing temperature, respectively (curves 2–5), and eventually, at 30 °C the component peak at ca. 500 nm was detected as a shoulder peak (curve 6). At 31 °C, the shape of the spectrum changed very slightly (curve 7). This spectral change appears to be brought about by the shift of the component peak at ca. 500 nm to slightly lower wavelengths. Taking into account the fact that the λ_{max} shift from 500 to 488 nm occurs at the pretransition in the pure DHPC membrane, this slight spectral change is presumably due to the pretransition of the binary membrane. The subsequent increase in the temperature up to 35 °C produced almost no change in the shape of the spectra, but above that temperature the intensities at 430 nm and 490 nm gradually decreased and increased with increasing temperature, respectively. The λ_{max} value abruptly shifted from ca. 430 to ca. 490 nm into the temperature range of 39–43 °C, and finally, the spectra with a single peak at ca. 490 nm were observed above 43 °C. Since the λ_{max} value of 490 nm is characteristic of a disordered phase like the L_α phase, this spectral change is attributable to the fact that the binary membrane underwent the main transition in this temperature range. On the other hand, there was no obvious variation in λ_{max} during the spectral change due to the pretransition, and so, the pretransition temperature could not be determined from the temperature dependence of λ_{max}. However, it can be estimated from the temperature dependence of the ratio of $F(430)/F(490)$, where the ratio reaches maximum in the vicinity of the temperature at which the spectral change due to the pretransition was observed.

At $X_{ch} = 0.077$, as shown in Fig. 5(b), the component peak at ca. 500 nm observed at lower temperatures was detected only as a small shoulder peak even at 5 °C and became further smaller with increasing temperature. However, the overall spectral change with increasing temperature observed for this binary membrane was qualitatively similar to that for the
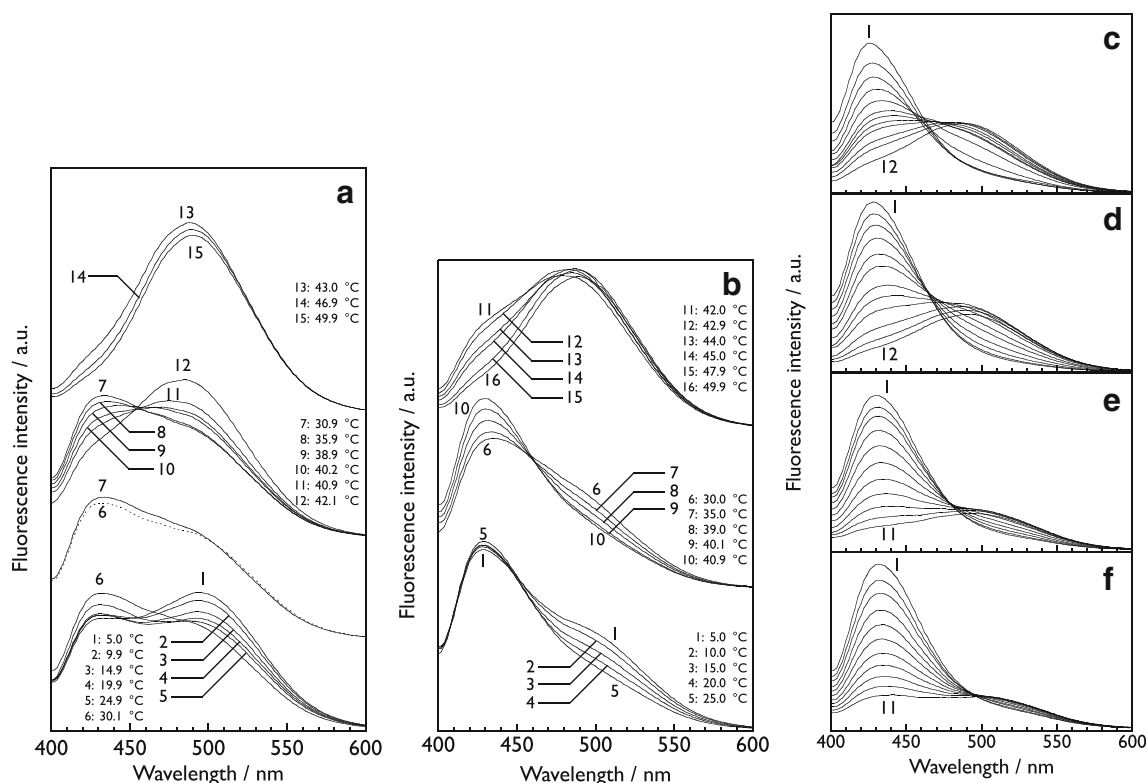
Fig. 5 Prodan emission spectra $F(\lambda)$ obtained at different temperatures for DHPC–Chol binary membranes at various Chol concentrations (X_{ch}): (a) $X_{ch} = 0.028$, (b) 0.077, (c) 0.15, (d) 0.24, (e) 0.40, (f) 0.54. Note that curves 6 and 7 in (a) are shown twice to clarify the spectral change accompanying the pretransition. The temperatures for curves in (c)–(f) are as follows: (c): (1) 5.0 °C, (2) 20.0, (3) 30.1, (4) 41.0, (5) 42.0, (6) 43.1, (7) 44.1, (8) 45.0, (9) 46.0, (10) 48.0, (11) 50.0, (12) 55.1; (d): (1) 30.0 °C, (2) 35.1, (3) 40.0, (4) 43.0, (5) 45.1, (6) 47.0, (7) 50.0, (8) 52.0, (9) 55.0, (10) 60.0, (11) 65.0, (12) 70.0; (e) and (f): each spectrum was obtained at every 5 ± 0.1 °C from (1) 30.0 °C to (11) 80.0 °C. In (c)–(f), only the first and the last number are given to designate the respective spectra because of the limited space, but the spectral change with temperature is monotonic (i.e., from top (1) to bottom (11 or 12))

binary membrane of $X_{ch} = 0.028$, though the spectral change by the pretransition could not be recognized. At $X_{ch} = 0.15$, the component peak at ca. 500 nm was no longer observed at any temperature (Fig. 5(c)), suggesting that the pretransition was completely abolished at this Chol concentration. In addition, the spectral change with increasing temperature became relatively simple: a spectrum with a single peak at ca. 430 nm was observed at 5 °C, the intensities at 430 and 490 nm decreased and increased gradually with increasing temperature, respectively, λ_{max} shifted to higher wavelengths in the temperature range of ca. 41–48 °C, and finally spectra with a single peak at ca. 490 nm were observed at temperatures above that temperature range. Similar spectral changes were observed for the binary membranes with higher Chol concentrations, as shown in Fig. 5(d, e), though the temperature range in which λ_{max} shifts from ca. 430 to ca. 490 nm moved to higher temperatures as X_{ch} increased. Finally, the λ_{max} shift to 490 nm was not observed at $X_{ch} = 0.54$ in the temperature range up to 80 °C (Fig. 5(f)), suggesting that the binary membrane no longer exhibits a distinct phase transition from an ordered state to a disordered state at that higher Chol concentration.

Figure 6 shows the temperature dependence of λ_{max} and $F(430)/F(490)$ in the temperature range of 20–80 °C for the DHPC–Chol binary membranes with various Chol concentrations. Although two local maxima were observed at ca. 430 and ca. 500 nm in the Prodan fluorescence spectra below 30 °C at $X_{ch} = 0.028$, we determined the λ_{max} value as a unique index according to the definition of λ_{max}. Therefore, the λ_{max} values for $X_{ch} = 0.028$ are approximately 430 nm in the temperature range between 20 and 30 °C in Fig. 6(a). After the λ_{max} value increased very slightly at 31 °C, it remained almost constant up to 37 °C, and then, it started to increase and reached almost 490 nm at 43 °C. The slight increase in λ_{max} at 31 °C corresponds to the slight spectral change due to the pretransition (see Fig. 5(a), curves 6 and 7), but this λ_{max} change is not a typical behavior of the pretransition of this binary membranes. In fact, no characteristic behavior of λ_{max} indicative of the pretransition was found in the temperature dependence of λ_{max} at any X_{ch} above 0.028, although it was indicated by the DSC results that the pretransition persists as high as $X_{ch} = 0.10$. This means that it is impossible to determine the pretransition temperature for the binary membranes at $X_{ch} > 0.028$ on the basis of the temperature

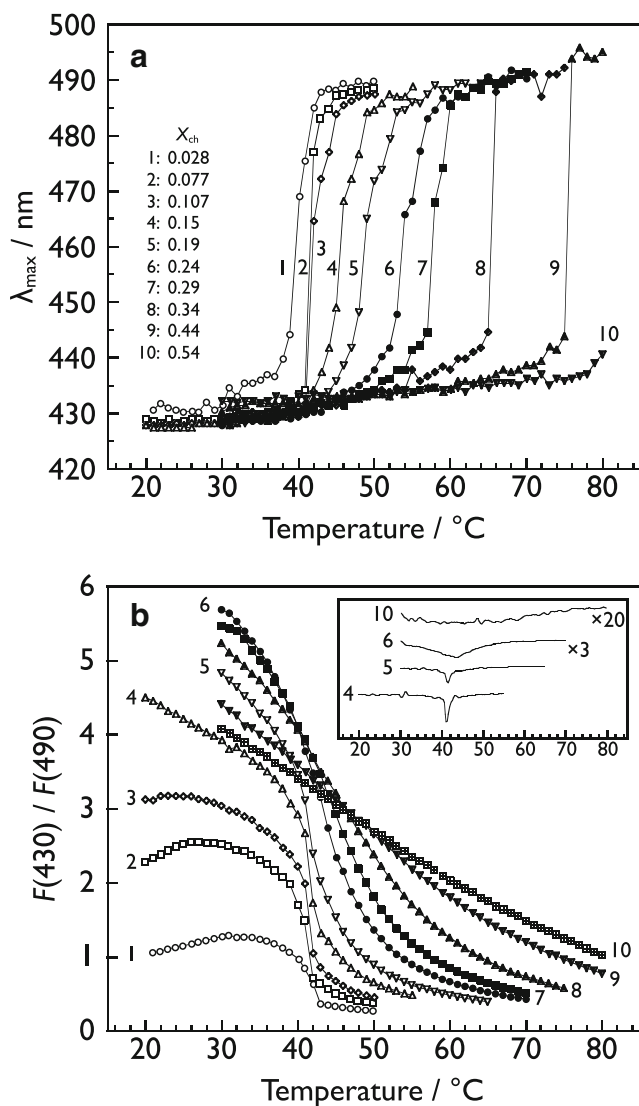**Fig. 6** Temperature dependence of (a) the wavelength at the maximum emission (λ_{max}) and (b) the intensity ratio $F(430)/F(490)$ for DHPC–Chol binary membranes at various Chol concentrations (X_{ch}). In the inset in (b), the temperature dependence curves of d($F(430)/F(490)$)/dT, i.e., the derivative of $F(430)/F(490)$ with respect to T, are given for (4) $X_{ch} = 0.15$, (5) 0.19, (6) 0.24, and (10) 0.54. Curves 6 and 10 have been magnified in the y-axis direction to improve visibility. The magnification factors are given on the right hand side

dependence curve of λ_{max}. On the other hand, the steep increase in λ_{max} to ca. 490 nm is a characteristic change observed commonly for many lipid bilayers when the main transition occurs. Therefore, this result indicates that the binary membrane of $X_{ch} = 0.028$ exists in a disordered state (i.e., L_d phase) above 43 °C.

At $X_{ch} = 0.077$, the abrupt λ_{max} shift was also clearly observed at 41 °C; subsequently, the λ_{max} value increased gradually with the temperature rise and finally reached the plateau at 45 °C. Almost similar behavior was observed at $X_{ch} = 0.11$, but the gradual increase in the λ_{max} value subsequent to the abrupt λ_{max} shift became more obvious, which seems to

indicate that the conversion from an ordered state to a disordered state is no longer a discontinuous change like a phase transition but a more continuous process taking place in a finite temperature range. At $X_{ch} = 0.15$, this process-like λ_{max} behavior can be seen more clearly: the λ_{max} value started to increase comparatively gradually at 42 °C and reached the plateau at ca. 49 °C through the abrupt change at 45 °C and the subsequent gradual increase. As seen from Fig. 6(a), the initial increase in λ_{max} prior to the abrupt λ_{max} shift became markedly more gradual with increasing X_{ch}, and as a result, the temperature at which the λ_{max} value reaches the plateau shifted considerably to higher temperatures with increasing X_{ch}. This means that the temperature range where the binary membrane can exist in a completely disordered state shifts to higher temperatures as X_{ch} increases. Finally, at $X_{ch} = 0.54$, the λ_{max} shift to ca. 490 nm was not observed in the temperature range up to 80 °C, which suggests that the binary membrane no longer exhibits the conversion from the ordered state to the disordered state at that higher Chol concentration. This is consistent with the DSC results which indicates that the DHPC–Chol binary membrane no longer exhibits the main transition above $X_{ch} = 0.50$.

The temperature dependence of the intensity ratio $F(430)/F(490)$ and its derivative d($F(430)/F(490)$)/dT also provides the information about the X_{ch}-dependent behavior of not only the main-transition temperature but also the pretransition temperature (Fig. 6(b)). At $X_{ch} = 0.028$, initially, the $F(430)/F(490)$ value increased gradually with increasing temperature and reached the maximum at 31 °C. This temperature is equal to the temperature at which the slight spectral change due to the pretransition was observed, and also comparable to the pretransition temperature determined from the DSC thermogram at $X_{ch} = 0.03$. This suggests that the pretransition temperature can be estimated from the temperature dependence of $F(430)/F(490)$ though the pretransition could not be clearly identified from the spectral change. As X_{ch} increased, the temperature at the maximum intensity ratio decreased, and finally, no maximum was found at an intermediate temperature at X_{ch} above ca. 0.12, which may suggest that the pretransition is abolished above that Chol concentration. This also agrees well with the DSC result which indicates that the pretransition is abolished above $X_{ch} = $ ca. 0.10.

On the other hand, the main transition was detected more clearly as a steep decrease in the intensity ratio. At $X_{ch} = 0.028$, the intensity ratio started to decrease gradually with increasing temperature after it reached the maximum, and a relatively steep decrease in the ratio was observed at 42–43 °C, which signifies that the binary membrane underwent the main transition around this temperature. This temperature was in agreement with the temperature determined from the temperature dependence of λ_{max} and that from the DSC

thermogram. The further increase in temperature above the main-transition temperature produced only a very slight decrease in the intensity ratio. The temperature of the steep decrease in the intensity ratio shifted very slightly to lower temperatures (at most 2 °C) with increasing X_{ch} up to ca. 0.06, but the further increase in X_{ch} produced virtually no effect on the temperature until X_{ch} exceeded 0.20. In addition, the decrease in the intensity ratio tended to be less steep progressively with increasing X_{ch}, and as a result, the intensity ratio decreased more continuously over the whole temperature range at higher X_{ch}, especially above ca. 0.20, which made it difficult or almost impossible to determine the transition temperature definitely. Hence, we computed the derivative of the intensity ratio with respect to the temperature, $d(F(430)/F(490))/dT$, to determine the transition temperature uniquely as a peak temperature, as shown in the inset of Fig. 6(b). The temperature dependence curve of the derivative exhibited a similar change in the line shape with increasing X_{ch} to that observed for a series of DSC thermograms.

Discussion

Effect of Chol incorporation on the formation of interdigitated structure

On the basis of the above DSC and Prodan fluorescence results, we can discuss the X_{ch}-dependent phase behavior of the DHPC–Chol binary membrane. Figure 7(a) shows the Prodan fluorescence spectra obtained at 20 °C (± 0.1 °C) for the binary membranes with different Chol concentrations within the X_{ch} range from 0 to 0.107. Each spectrum shown in this figure is the normalized spectrum $F^\circ(\lambda)$ with respect to the integrated intensity:

$$F^\circ(\lambda) = \frac{F(\lambda)}{\int_{400}^{600} F(\lambda)\,d\lambda} \tag{3}$$

It can be clearly seen that the peak intensity at 500 nm decreases and that at 430 nm increases with increasing X_{ch}. Since these wavelengths correspond to the λ_{max} value characteristic of the membrane phase states of $L_\beta I$ and L_β, this X_{ch}-dependent spectral change can be considered to indicate that the conversion from the $L_\beta I$ phase to the L_β phase gradually proceeds with increasing X_{ch} and is almost completed at $X_{ch} = 0.107$ and that the $L_\beta I$ and the L_β phase coexist within the binary membrane at intermediate Chol concentrations within this X_{ch} range. The previous small-angle X-ray scattering study [21] has also demonstrated that two different regions with different thicknesses (i.e., interdigitated and non-
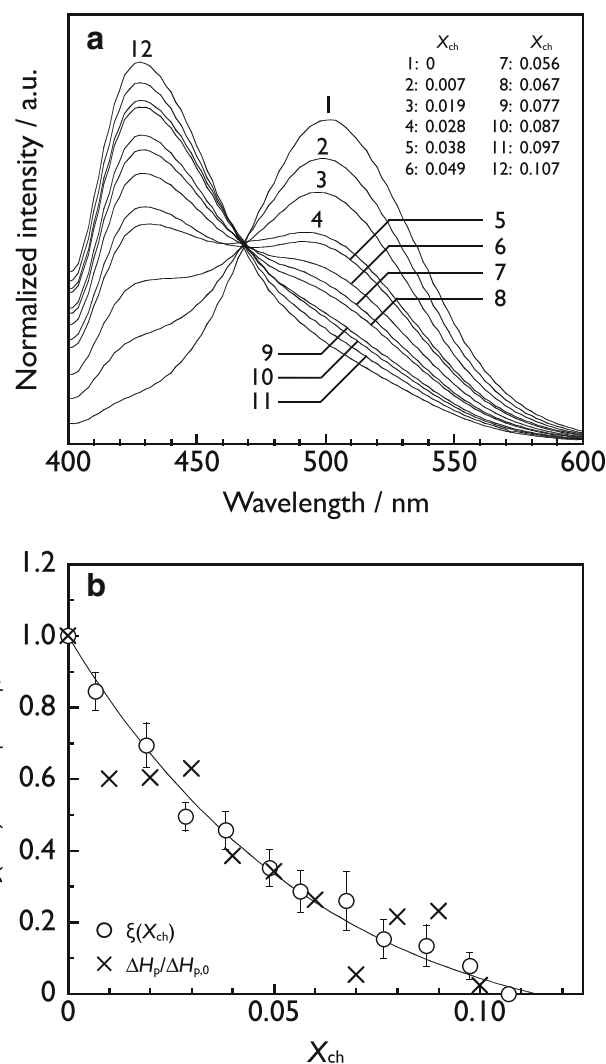

Fig. 7 (a) Normalized spectra of Prodan fluorescence for a series of DHPC–Chol binary membranes varying in Chol concentration (X_{ch}). (b) Chol concentration (X_{ch}) dependence of proportionality factor $\xi(X_{ch})$ (circles). Relative enthalpy change with the pretransition $\Delta H_p / \Delta H_{p,0}$, obtained from DSC measurements, is also plotted as a function of X_{ch} (crosses). The solid line represents the theoretical curve of Eq. (7) with $K_1 = 19$ and $K_2 = 2.2$

interdigitated lamellar gel phase) coexist in the Chol-containing binary membrane of DHPC at low Chol concentrations. With respect to this two-phase coexistence, this figure shows another important feature: there is an isoemissive point at ca. 468 nm, namely the point at which all the spectra cross one another. This feature indicates the possibility that each spectrum can be represented as the superposition of the spectra at $X_{ch} = 0$ and 0.107 with a proportionality factor $\xi(X_{ch})$ ($0 \leq \xi(X_{ch}) \leq 1$):

$$F^\circ(\lambda, X_{ch}) = \xi(X_{ch}) F^\circ(\lambda, 0) + [1 - \xi(X_{ch})] F^\circ(\lambda, 0.107) \tag{4}$$

Considering this possibility, we compared the calculated spectra based on this equation with the experimental spectra and found that the relative difference between both spectra is less

than ca. 5%. This agreement means that the observed X_{ch}-dependent spectral change is due only to the variation in the proportionality factor, which allows us to discuss the X_{ch}-dependent conversion from the $L_\beta I$ phase to the L_β phase from a quantitative aspect.

A similar X_{ch}-dependent spectral change was observed at any temperature measured in the range of 5–30 °C, and thus we determined the $\xi(X_{ch})$ value at each X_{ch} as the average value of all the $\xi(X_{ch})$ values obtained in this temperature range. In Fig. 7(b), the $\xi(X_{ch})$ value thus determined are plotted against X_{ch}. In this figure, the error bars represent the full range of the variation in the $\xi(X_{ch})$ values within that temperature range. The $\xi(X_{ch})$ value decreased monotonically with increasing X_{ch} in such a manner that the slope of the decrease in $\xi(X_{ch})$ becomes smaller with increasing X_{ch}. Assuming that the distribution of the Prodan molecules within the binary membrane is uniform regardless of the membrane phase state [32], the $\xi(X_{ch})$ value can be regarded as equivalent to the ratio occupied by the $L_\beta I$ phase in the whole binary membrane. Therefore, this behavior of $\xi(X_{ch})$ indicates that the $L_\beta I/L_\beta$ conversion induced by the incorporation of Chol gradually diminishes as X_{ch} increases. In Fig. 7(b), $\Delta H_p/\Delta H_{p,0}$, namely enthalpy change of the pretransition (i.e., ΔH_p) normalized by that at $X_{ch} = 0$ (i.e., $\Delta H_{p,0}$), is also plotted against X_{ch}. Similar X_{ch} dependence was seen for $\Delta H_p/\Delta H_{p,0}$, though the plots were somewhat scattered. Since ΔH_p is the enthalpy change accompanying the transformation of the membrane state from the $L_\beta I$ phase to the P_{β}' phase, this X_{ch} dependence of $\Delta H_p/\Delta H_{p,0}$ also supports that the region occupied by the $L_\beta I$ phase decreases with increasing X_{ch} in a similar non-linear manner.

This non-linear behavior of the Chol-induced $L_\beta I/L_\beta$ conversion can be roughly explained by a simple process of the Chol incorporation based on the following three assumptions. First, when a small amount of Chol is incorporated into the binary membrane in a two-phase state at a certain X_{ch}, the additional Chol molecules are partitioned into either $L_\beta I$ or L_β region without any phase preference, and the amounts of the Chol incorporated into the $L_\beta I$ and the L_β region are proportional to $\xi(X_{ch})$ and $(1 - \xi(X_{ch}))$, respectively. Second, the Chol molecules partitioned into the $L_\beta I$ region induce the conversion from the $L_\beta I$ state to the L_β phase and the extent of the $L_\beta I/L_\beta$ conversion is in proportion to the amount of Chol partitioned at any X_{ch}. Third, the Chol molecules partitioned into the L_β region expand the L_β region in proportion to the amount of Chol partitioned at any X_{ch}. According to this simple probabilistic process for the Chol incorporation, the variation in $\xi(X_{ch})$ with a small increment in Chol molecules (dn_{ch}) can be described by the following equation:

$$-d\xi(X_{ch}) = k_1 \xi(X_{ch}) dn_{ch} + k_2 [1 - \xi(X_{ch})] dn_{ch} \qquad (5)$$

Here, k_1 and k_2 denote the proportional constants in the second and the third assumption, respectively. Since the following

relation is obtained by differentiating Eq. (1)

$$dn_{ch} = \frac{n_{DHPC}}{(1 - X_{ch})^2} dX_{ch} \qquad (6)$$

$\xi(X_{ch})$ can be expressed as a function of X_{ch} as follows:

$$\xi(X_{ch}) = \frac{K_1}{K_1 - K_2} \exp\left[-(K_1 - K_2)\frac{X_{ch}}{1 - X_{ch}}\right] - \frac{K_2}{K_1 - K_2} \qquad (7)$$

Here, $K_1 = n_{DHPC}k_1$ and $K_2 = n_{DHPC}k_2$. Note that in this process, n_{DHPC} is constant and that the constants K_1 and K_2 are dimensionless. The calculated curve of $\xi(X_{ch})$ based on this equation with $K_1 = 19$ and $K_2 = 2.2$ is shown by a solid line in Fig. 7(b). The calculated curve agrees well with the experimental data, which provides us with quantitative information about the Chol-induced $L_\beta I/L_\beta$ conversion. First, the tangent line at $X_{ch} = 0$ intersects with the X_{ch}-axis at $X_{ch} = 0.0526$ (= 1/K_1). This means that the first Chol molecule incorporated into the DHPC membrane, which is entirely in the $L_\beta I$ state, has the $L_\beta I/L_\beta$ conversion effect on 18 DHPC molecules around the Chol molecule. Second, the calculated curve of $\xi(X_{ch})$ becomes 0 at $X_{ch} = 0.114$. This Chol concentration approximately corresponds to the average molar ratio of 1:8 (Chol/DHPC), and thus, the average molar ratio of Chol in the overall L_β region increases continuously from 1:18 at $X_{ch} \sim 0$ to ca. 1:8 at $X_{ch} = 0.114$ as X_{ch} increases. If the process of Chol incorporation we assumed is true, the distribution of the Chol molecules in the overall L_β region will be heterogeneous at intermediate X_{ch}. As expected from the K_1 and the K_2 value, the Chol molecules incorporated into the L_β region and those into the $L_\beta I$ region make different contributions to the expansion of the overall L_β region, and thus, there can exist microregions or microdomains of the L_β phase with different molar ratios of Chol within the whole binary membrane. Finally, when the entire binary membrane is occupied by the L_β region at $X_{ch} = 0.114$, the binary membrane totally becomes a bilayer and no longer undergoes the pretransition.

T–X_{ch} phase diagram of DHPC–Chol binary membrane

We now discuss the overall phase behavior of the DHPC–Chol binary membrane. Figure 8(a) shows the T–X_{ch} phase diagram of the DHPC–Chol binary membrane constructed on the basis of the DSC data (i.e., peak temperature) and the Prodan fluorescence data. For comparison, the T–X_{ch} phase diagram of DPPC–Chol binary bilayer reported in the previous study [15] is also shown in Fig. 8(b). In the previous study [15], we interpreted the phase diagram of the DPPC–Chol binary bilayer on the basis of the general thermodynamic knowledge about the solid/liquid phase equilibria of peritectic
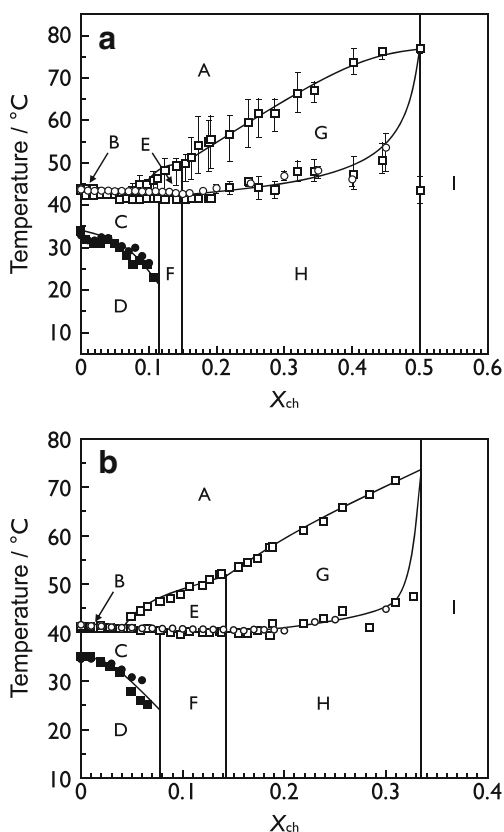
Fig. 8 (a) Temperature (T)–Chol concentration (X_{ch}) phase diagram of DHPC–Chol binary membrane. Phase assignment is as follows: (A) L_d phase, (B) L_d + P_{β}', (C) P_{β}' + L_{β} (1:8), (D) $L_{\beta}I$ + L_{β} (1:8), (E) L_d + L_{β} (1:6), (F) L_{β} (1:8) + L_{β} (1:6), (G) L_d + L_o, (H) L_{β} (1:6) + L_o, (I) L_o. Here, the plus sign means the two-phase coexistence. (b) T–X_{ch} phase diagram of DPPC–Chol binary bilayer constructed in our previous study [15] is also shown for comparison. Phase assignment is the same as above except the followings: (C) P_{β}' + L_{β} (1:12), (D) L_{β}' + L_{β} (1:12), (F) L_{β} (1:12) + L_{β} (1:6). Circle and square symbols represent the data from the DSC and the Prodan fluorescence measurements, respectively

binary mixtures. We applied the same thermodynamic concept to the phase diagram of the DHPC–Chol binary membrane to perform the phase assignment: A, L_d phase; B, L_d + P_{β}'; C, P_{β}' + L_{β} (1:8); D, $L_{\beta}I$ + L_{β} (1:8); E, L_d + L_{β} (1:6); F, L_{β} (1:8) + L_{β} (1:6); G, L_d + L_o; H, L_{β} (1:6) + L_o; I, L_o. Here, the plus sign means two-phase coexistence. The ratio in parentheses denotes the average molar ratio of Chol to DHPC, and the L_{β} (1:8) phase and the L_{β} (1:6) phase are considered to be thermodynamically different phases.

As a common feature, the phase diagrams of these binary membranes suggest the presence of a characteristic point like a peritectic point at X_{ch} = ca. 0.15. In general, a peritectic point occurs as a result of incongruent melting, and this type of melting behavior is usually observed for binary systems where the two components react to produce a solid compound with a specific stoichiometry that is stable in a solid state but unstable in a liquid state. It is therefore suggested that the Chol

molecules tend to form complexes or molecular clusters with surrounding DHPC molecules within the binary membrane. In addition, the stoichiometry of the complex is estimated at 1:6 (Chol/DHPC) from the fact that the peculiar point like a peritectic point was observed at X_{ch} = ca. 0.15 (the ratio of 1:6 is equivalent to X_{ch} = 0.143). The same result has been also found for the other Chol-containing binary bilayers of CnPC (n = 14, 15, 17, 18) [13–15]. This is very interesting because it is expected that the strength or mode of the interaction between the Chol and constituent phospholipid molecules should more or less change when the molecular structure of the constituent phospholipid varies. It has been reported that Chol molecules tend to be distributed regularly within the binary bilayer of CnPCs [33–35] and the distribution is well represented with the hexagonal lattice (i.e., superlattice view [16]). Accordingly, the 1:6 complexes of Chol and phospholipids would be a weak unit occurring as a result of the regular distribution of Chol within the binary membrane rather than a rigid complex resulting from some specific or more direct Chol–phospholipid interaction.

On the other hand, the phase behavior of the DHPC– and the DPPC–Chol binary membrane is different in respect of the minimum Chol concentration at which the L_o phase is formed as a single phase throughout the binary membrane: X_{ch} = ca. 0.5 for DHPC and X_{ch} = ca. 0.33 for DPPC. The L_o phase is often characterized as the membrane state where the chain-melting transition no longer occurs and this is thought to be due to the suppression of the *trans–gauche* conformational change in the hydrocarbon chains of the constituent phospholipids by the rigid Chol molecules existing adjacent to them. Accordingly, the minimum X_{ch} value of the entire formation of the L_o phase is equivalent to $X_{ch}*^{main}$. In the previous study [15], the same difference in the $X_{ch}*^{main}$ value was observed between the binary bilayer of DSPC (i.e., C18PC) and those of the other CnPCs (n = 14–17). We speculated that this difference is attributable to the mismatch in the effective length of the hydrophobic region between Chol and the constituent phospholipid in the binary membrane on the basis of the fact that the hydrophobic mismatch is minimized at the chain length of 17 [31, 36].

The difference in the $X_{ch}*^{main}$ value between the binary membranes of DHPC and DPPC could also be explained in terms of the hydrophobic mismatch at the bilayer midplane, although the hydrocarbon-chain length of DHPC is equal to that of DPPC. It has been reported that the Chol molecules reside within the bilayer such that their hydrophobic part (i.e., the four sterol rings and the side chain) is buried into the hydrophobic core of the bilayer with its 3β-OH group protruding into the hydrophilic region of the bilayer [37–39]. In the case that the constituent phospholipid is DPPC, this position of the Chol molecule in the depth direction within the

bilayer is expected to be stabilized by hydrogen bonding between the 3β-OH group and the carbonyl oxygen at the glycerol backbone of an adjacent DPPC molecule. Meanwhile, in the case of DHPC, it is expected that the Chol molecule could alter its vertical position within the membrane relatively less restrictedly as compared to the case of the DPPC bilayer, because DHPC is not capable of hydrogen bonding with the 3β-OH group of the neighboring Chol molecule at the glycerol backbone owing to the absence of carbonyl oxygens. Consequently, the effect of the hydrophobic mismatch at the bilayer midplane is expected to be more or less reduced in the DHPC membrane, which would result in the higher $X_{\mathrm{ch}}^{*\mathrm{main}}$ value. This would be supported by the DSC data suggesting that the Chol–phospholipid interaction is weaker within the binary membrane of DHPC than within that of DPPC (or DSPC).

In the last place, we discuss the comparison with a phase diagram of the same system given in the previous study by Laggner et al. [21]. Their phase diagram was also constructed on the basis of DSC data, but the phase boundary was determined as the onset and the completion temperatures of the main-transition endothermic peaks. The loop-like boundary thus obtained was explained from the viewpoint of a typical liquid–liquid phase separation due to a miscibility gap. This explanation logically implies that DHPC and Chol are miscible within the binary membrane to form a homogeneous phase even in the gel state (i.e., below the main-transition temperature). In fact, there is no indication about the phase states in their phase diagram, although the phase boundaries of the pretransition and even the subtransition (i.e., transition from the lamellar crystal (L_c) phase to the $L_\beta I$) are provided. Therefore, our phase diagram, suggesting solid–liquid phase equilibria, is utterly different from their phase diagram. In other words, the major difference between their and our phase diagram would arise from the difference in the thermodynamic interpretation of the phase behavior of the binary membrane rather than from the experimental results themselves.

This is evident from the fact that our phase diagram looks more similar to the phase diagram re-constructed by Marsh [17] in his comprehensive work, which is based on the same data reported in the original study by Laggner et al. [21]. His re-constructed phase diagram suggests that the DHPC–Chol binary membrane basically exhibits eutectic melting behavior, and then, there are several two-phase states in the gel state depending on the Chol concentration, which is similar to our phase diagram. The essential difference between his and our phase diagram lies in the difference of whether the melting behavior that the binary membrane exhibits is eutectic or peritectic, as long as some quantitative differences are ignored. In this regard, we need to perform further investigation to obtain more direct or strong evidence for the presence of the

1:6 complex of Chol and DHPC within the binary membrane that we propose on the basis of the present and our previous studies on the Chol-containing binary membranes [13–15].

Conclusions

In this study, we performed DSC and Prodan fluorescence spectroscopic measurements to investigate the thermotropic phase behavior of the DHPC–Chol binary membrane as a function of X_{ch}. The DSC measurements demonstrated that the thermal behavior of the DHPC–Chol binary membrane is different in several respects compared to that of the DPPC–Chol binary bilayer. First, the main-transition enthalpy decreased to 0 at X_{ch} = ca. 0.50 for the DHPC–Chol binary membrane, while it decreased almost linearly with increasing X_{ch} and reached 0 at X_{ch} = ca. 0.33 for the DPPC–Chol binary bilayer. This X_{ch} dependence of ΔH_{m} for the DHPC–Chol binary membrane suggests weaker interaction between DHPC and Chol as compared to that between DPPC and Chol. Second, the increase in $\Delta T_{1/2}$ with increasing X_{ch} above ca. 0.15 was strikingly larger than that observed for the DPPC–Chol binary bilayer. This difference would reflect the difference in the long-range order of the membrane lateral organization between the DHPC– and the DPPC–Chol binary membrane. Prodan fluorescence spectroscopy was successfully applied to the observation of the phase transitions of the DHPC–Chol binary membranes. The Prodan fluorescence spectra changed depending on the membrane phase states, and the spectral change was basically characterized by the λ_{max} value and the intensity ratio of $F(430)/F(490)$. Particularly, the two-phase state of the $L_\beta I$ and the Chol-induced L_β phase could be sensitively detected as the superposition of the two elementary spectra corresponding to the respective phase states. By introducing a proportionality factor $\xi(X_{\mathrm{ch}})$, we could analyze the X_{ch}-dependent spectral change due to the $L_\beta I/L_\beta$ conversion induced by the Chol incorporation, and we found that the incorporation of Chol into the binary membrane in the two-phase state can be explained as a simple probabilistic process. Our calculation revealed that in this process, one Chol molecule incorporated into the $L_\beta I$ region has the effect of inducing the L_β region on its surrounding 18 DHPC molecules.

On the basis of the DSC and Prodan fluorescence data, we constructed the T–X_{ch} phase diagram for the DHPC–Chol binary membrane to compare it with that of the DPPC–Chol binary membrane. A difference was observed in the minimum X_{ch} value for the entire formation of the L_o phase. This difference could be explained in terms of the hydrophobic mismatch at the bilayer midplane. We can finally conclude that the degree or extent of the Chol effect on the membrane phase behavior is pronouncedly affected by the difference in the

chemical structure between DHPC and DPPC, namely the difference in the capability of hydrogen bonding with the 3β-OH group of Chol due to the presence or absence of the carbonyl oxygens at the glycerol backbone.

Compliance with ethical standards

Conflict of interest The authors declare that they have no conflict of interest.

References

1. Lewis RNAH, Mak N, McElhaney RN (1987) A differential scanning calorimetric study of the thermotropic phase behavior of model membranes composed of phosphatidylcholines containing linear saturated fatty acyl chains. Biochemistry 26:6118–6126

2. Ichimori H, Hata T, Matsuki H, Kaneshina S (1998) Barotropic phase transitions and pressure-induced interdigitation on bilayer membranes of phospholipids with varying acyl chain-lengths. Biochim Biophys Acta 1414:165–174

3. Ruocco MJ, Siminovitch DJ, Griffin RG (1985) Comparative study of the gel phases of ether- and ester-linked phosphatidylcholines. Biochemistry 24:2406–2411

4. Laggner P, Lohner K, Degovics G, Müller K, Schuster A (1987) Structure and thermodynamics of the dihexadecylphosphatidylcholine–water system. Chem Phys Lipids 44:31–60

5. Koynova R, Koumanov A, Tenchov B (1996) Metastable ripple gel phase in saturated phosphatidylcholines: calorimetric and densitometric characterization. Biochim Biophys Acta 1285:101–108

6. Maruyama S, Matsuki H, Ichimori H, Kaneshina S (1996) Thermotropic and barotropic phase behavior of dihexadecylphosphatidylcholine bilayer membrane. Chem Phys Lipids 82:125–132

7. Kim JT, Mattai J, Shipley GG (1987) Gel phase polymorphism in ether-linked dihexadecylphosphatidylcholine bilayers. Biochemistry 26:6592–6598

8. Gawrisch K, Ruston D, Zimmerberg J, Parsegian A, Rand RP, Fuller N (1992) Membrane dipole potentials, hydration forces, and the ordering of water at membrane surfaces. Biophys J 61: 1213–1223

9. Matsuki H, Miyazaki E, Sakano F, Tamai N, Kaneshina S (2007) Thermotropic and barotropic phase transitions in bilayer membranes of ether-linked phospholipids with varying alkyl chain lengths. Biochim Biophys Acta 1768:479–489

10. Simons K, Ikonen E (1997) Functional rafts in cell membranes. Nature 387:569–572

11. Ipsen JH, Karlström G, Mouritsen OG, Wennerström H, Zuckermann MJ (1987) Phase equilibria in the phosphatidylcholine–cholesterol system. Biochim Biophys Acta 905:162–172

12. Vist MR, Davis JH (1990) Phase equilibria of cholesterol/dipalmitoylphosphatidylcholine mixtures: ^{2}H nuclear magnetic resonance and differential scanning calorimetry. Biochemistry 29: 451–464

13. Tamai N, Uemura M, Takeichi T, Goto M, Matsuki H, Kaneshina S (2008) A new interpretation of eutectic behavior for distearoylphosphatidylcholine–cholesterol binary bilayer membrane. Biophys Chem 135:95–101

14. Tamai N, Uemura M, Goto M, Matsuki H, Kaneshina S (2008) Lateral phase separation in cholesterol/diheptadecanoylphosphatidylcholine binary bilayer membrane. Colloids Surf B Biointerfaces 65:213–219

15. Tamai N, Izumikawa T, Fukui S, Uemura M, Goto M, Matsuki H, Kaneshina S (2013) How does acyl chain length affect thermotropic phase behavior of saturated diacylphosphatidylcholines–cholesterol binary bilayers? Biochim Biophys Acta 1828:2513–2523

16. Somerharju P, Virtanen JA, Cheng KH (1999) Lateral organisation of lipids: the superlattice view. Biochim Biophys Acta 1440:32–48

17. Marsh D (2010) Liquid-ordered phases induced by cholesterol: a compendium of binary phase diagrams. Biochim Biophys Acta 1798:688–699

18. Chong PLG (1988) Effects of hydrostatic pressure on the location of PRODAN in lipid bilayers and cellular membranes. Biochemistry 27:399–404

19. Kusube M, Matsuki H, Kaneshina S (2005) Effect of pressure on the Prodan fluorescence in bilayer membranes of phospholipids with varying acyl chain lengths. Colloids Surf B Biointerfaces 42:79–88

20. Hénin J, Chipot C (2006) Hydrogen-bonding patterns of cholesterol in lipid membranes. Chem Phys Lett 425:329–335

21. Laggner P, Lohner K, Koynova R, Tenchov B (1991) The influence of low amounts of cholesterol on the interdigitated gel phase of hydrated dihexadecylphosphatidylcholine. Chem Phys Lipids 60:153–161

22. Kusube M, Goto M, Tamai N, Matsuki H, Kaneshina S (2007) Effect of pressure on the Prodan fluorescence in bilayer membrane of ether-linked lipid, dihexadecylphosphatidylcholine. High Press. Biosci. Biotechnol.: Proc. 4th Int. Conf. High Press. Biosci. Biotechnol 1:61–67

23. Yeagle PL (2005) The roles of cholesterol in the biology of cells. In: Yeagle PL (ed) The structure of biological membrane 2nd edn. CRC Press, London Chapter 2

24. Dufourc EJ, Parish EJ, Chitrakorn S, Smith ICP (1984) Structural and dynamical details of cholesterol-lipid interaction as revealed by deuterium NMR. Biochemistry 23:6062–6071

25. Tsong TY (1974) Kinetics of the crystalline–liquid crystalline phase transition of dimyristoyl L-α-lecithin bilayers. Proc Natl Acad Sci U S A 71:2684–2688

26. Kusube M, Tamai N, Matsuki H, Kaneshina S (2005) Pressure-induced phase transitions of lipid bilayers observed by fluorescent probes Prodan and Laurdan. Biophys Chem 117:199–206

27. Goto M, Kusube M, Tamai N, Matsuki H, Kaneshina S (2008) Effect of hydrostatic pressure on the bilayer phase behavior of symmetric and asymmetric phospholipids with the same total chain length. Biochim Biophys Acta 1778:1067–1078

28. Goto M, Sawaguchi H, Tamai N, Matsuki H, Kaneshina S (2010) Effect of vesicle size on the prodan fluorescence in diheptadecanoylphosphatidylcholine bilayer membrane under atmospheric and high pressure. Langmuir 26:13377–13384

29. Goto M, Matsui T, Tamai N, Matsuki H, Kaneshina S (2011) Prodan fluorescence detects the bilayer packing of asymmetric phospholipids. Colloids Surf B Biointerfaces 84:55–62

30. Goto M, Wilk A, Kataoka K, Chodankar S, Tamai N, Fukui M, Kohlbrecher J, Ito H, Matsuki H (2012) Study on the subgel-phase formation using an asymmetric phospholipid bilayer membrane by high-pressure fluorometry. Langmuir 28:12191–12198

31. McMullen TPW, Lewis RNAH, McElhaney RN (1993) Differential calorimetric study of the effect of cholesterol on the thermotropic phase behavior of a homologous series of linear saturated phosphatidylcholine. Biochemistry 32:516–522

32. Matsuki H, Kato K, Okamoto H, Yoshida S, Goto M, Tamai N, Kaneshina S (2017) Ligand partitioning into lipid bilayer membranes under high pressure: implication of variation in phase-transition temperatures. Chem Phys Lipids 209:9–18

33. Chong PLG (1994) Evidence for regular distribution of sterols in liquid crystalline phosphatidylcholine bilayers. Proc Natl Acad Sci U S A 91:10069–10073

34. Tang D, van der Meer BW, Chen SYS (1995) Evidence for a regular distribution of cholesterol in phospholipid bilayers from diphenylhexatriene fluorescence. Biophys J 68:1944–1951

35. Virtanen JA, Ruonala M, Vauhkonen M, Somerharju P (1995) Lateral organization of liquid-crystalline cholesterol–dimyristoylphosphatidylcholine bilayers. Evidence for domains with hexagonal and centered rectangular cholesterol superlattices. Biochemistry 34:11568–11581

36. McIntosh TJ (1978) The effect of cholesterol on the structure of phosphatidylcholine bilayers. Biochim Biophys Acta 513:43–58

37. Karolis C, Coster HGL, Chilcott TC, Barrow KD (1998) Differential effects of cholesterol and oxidised-cholesterol in egg lecithin bilayers. Biochim Biophys Acta 1368:247–255

38. Bhattacharya S, Haldar S (2000) Interactions between cholesterol and lipids in bilayer membranes. Role of lipid headgroup and hydrocarbon chain–backbone linkage. Biochim Biophys Acta 1467: 39–53

39. Khelashvili G, Pabst G, Harries D (2010) Cholesterol orientation and tilt modulus in DMPC bilayers. J Phys Chem B 114:7524–7534